International Journal of Mass Spectrometry 308 (2011) 41–48

Contents lists available at ScienceDirect

International Journal of Mass Spectrometry

journal homepage: www.elsevier.com/locate/ijms

Relation between charge state distributions of peptide anions and pH changes in the electrospray plume. A mass spectrometry and optical spectroscopy investigation

Marion Girod[a,b,c], Xavier Dagany[a,b,c], Rodolphe Antoine[a,b,c,*], Philippe Dugourd[a,b,c]

[a] Université de Lyon, F-69622, Lyon, France
[b] Université Lyon 1, Villeurbanne, France
[c] CNRS, UMR5579, LASIM, France

ARTICLE INFO

Article history:
Received 13 June 2011
Received in revised form 13 July 2011
Accepted 13 July 2011
Available online 4 August 2011

Keywords:
Electrospray
Fluorescence
Peptides
Profiling
Charge state distribution

ABSTRACT

A laser-induced fluorescence set-up profiling physico-chemical parameters of droplets and their changes in an electrospray plume is coupled to an Agilent single quadrupole mass spectrometer equipped with an Agilent Jet Stream electrospray source. This coupling allows investigating the evolution of the pH of droplets as they evaporate in the electrospray plume by measuring emission spectra of a pH-chromic dye. Simultaneous measurement of mass spectra and optical pH profiling permits to study the relation between the charge states of peptide anions in mass spectra and pH changes in the spray plume. In particular, due to changes in droplets evaporation rates, the source parameters (i.e., sheath gas flow and temperature) influence the pH of the droplets and relative intensities of charge states in peptide mass spectra.

1. Introduction

Electrospray ionization (ESI) mass spectrometry (MS) has evolved into one of the most versatile and widely used analytical techniques. It allows the transfer of macromolecules into the gas phase as intact ions [1], and has emerged in recent years as an indispensable tool for the study of biological macromolecules in the gas phase [2]. The plume between the electrospray emitter and the sampling orifice of the mass spectrometer is a region that drives the entire desolvation process. Electrochemical aspects are well understood [3,4], but only a phenomenological understanding of evaporation mechanisms is available [5]. A fundamental understanding of the mechanistic details along the spray plume is required in particular to further improve the ionization efficiency, the sensitivity and the stability of these ion sources.

Directly probing the ESI plume between the electrospray emitter and the sampling orifice of the mass spectrometer is the key-feature in order to get the dynamics of ESI droplets during the evaporation process. Fenn and coworkers [6] have developed a sampling device that can be inserted into the plume at various locations. Using this device, they were able to observe solvent fractionation during the evaporation of charged droplets. In parallel, spectroscopic measurements can help to investigate the chemical and physical properties of electrospray droplets within the spray stream. As compared to mechanical techniques, optical methods have the main advantages to be non-intrusive, and hence allow both optical and mass spectrometry characterization of the electrospray. Pioneering works were performed by Van Berkel and coworkers [7] who measured the fluorescence excitation spectra of the octaethylporphyrin analyte in the electrospray stream. Cook and coworkers [8–11] and more recently Zenobi and coworkers [12–14] developed different laser-induced fluorescence strategies to probe chemical properties, for instance solvent fractionation, solvent polarity and the pH of electrospray droplets within the spray stream.

Spectroscopic measurements were used to probe the conformation and structural changes that biomolecules undergo during their transfer from the solution to the gas phase. The acid induced denaturation of cytochrome c protein was studied by Konermann and Douglas [15] using optical measurements in solution and mass spectrometry in order to investigate the relationship between the solution protein conformation and charge state distributions observed in the final ESI mass spectra. More recently, Parks and colleagues [16] and Ideue et al. [17] used dispersed fluorescence of tryptophan containing proteins to characterize spray-induced changes in protein conformations. However, these previous experiments were performed with mimic electrospray sources (i.e., ESI

* Corresponding author at: LASIM UMR 5579 CNRS & UNI LYON1, Bât. A. KASTLER, 43 bd du 11 novembre 1918, Villeurbanne, France. Fax: +33 4 72 43 15 07.
E-mail address: rantoine@lasim.univ-lyon1.fr (R. Antoine).

1387-3806/$ – see front matter © 2011 Elsevier B.V. All rights reserved.
doi:10.1016/j.ijms.2011.07.020

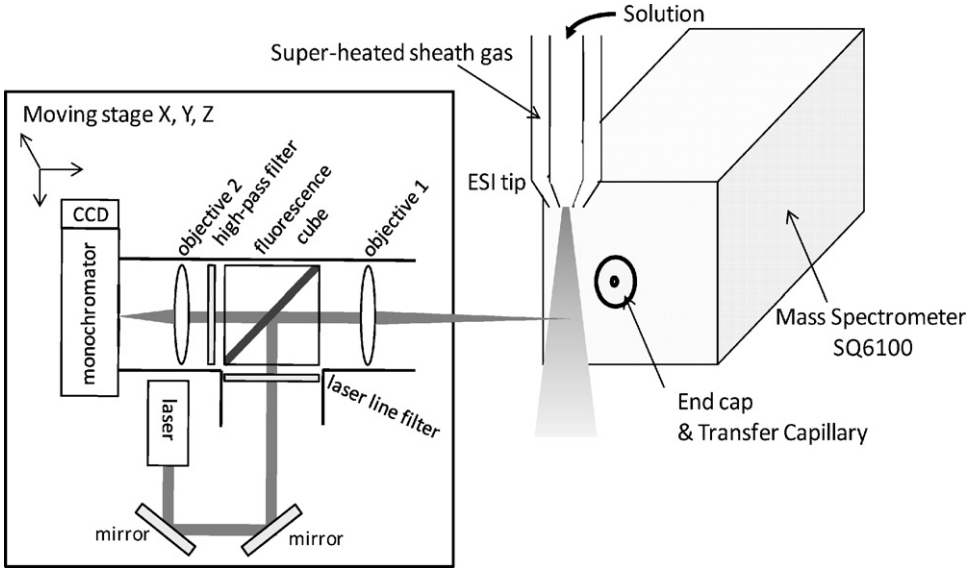

Fig. 1. Schematic diagram of the experimental setup used to probe fluorescence in the Agilent Jet Stream plume.

capillary and counter electrode) without simultaneous MS measurements of charge state distributions.

The complex dynamics of the ESI process make the transition from solution-phase to gas-phase ions difficult to model. Therefore, the correlation between the ions in the initial sample solution and those ions observed in the gas-phase by the mass spectrometer, can take advantage of direct optical spectroscopic measurements of physico-chemical parameters of droplets and their changes in the electrospray plume. Based on the current state-of-the-art imaging of sprays, we propose a new experimental approach that combines laser-induced fluorescence with mass spectrometry measurements. For this purpose we implemented a laser-induced-fluorescence profiling set-up on a modified Agilent Jet Stream electrospray source coupled to a single quadrupole mass analyser. The optical set-up permits to profile the pH of the droplets as they evaporate in an electrospray plume by measuring emission spectra of a pH-sensitive fluorescent dye and to record simultaneously mass spectra. This mass spectrometry and optical spectroscopy investigations allow studying the relation between the observed charge state of peptide anions and pH changes in the spray plume.

2. Experimental

2.1. Optical instrumentation

The experimental setup profiling the spray plume consists of an excitation laser and an optical detection system mounted on a moving stage. It is coupled to a single quadrupole mass spectrometer equipped with an electrospray ionization source (Fig. 1). An Oxxius Slim 532-300 (Oxxius Inc., Santa Clara, CA, USA) has been used for excitation of fluorescent dyes in the ESI plume. This is a 532 nm cw laser emitting in a single longitudinal mode. The output power of the laser is 300 mW and its beam diameter is 0.3 mm (divergence 1.2 mrad). The laser is injected through a fluorescence cube using two reflecting protected aluminum flat mirrors ($R > 90\%$).

In order to focus the laser beam into the spray and collect the fluorescence, an Optem 125C objective (Thales Optem Inc., Fairport, NY, USA) is used in an epi-fluoresence configuration. This objective consists of a zoom module and a 15 mm fine focus manual with a working distance of 89 mm. A long working distance was required due to the bulkiness of the ESI source block. A fluorescence cube, consisting of a dichroic mirror (BightLine Di01-R532-25x36, Optoprim, Vanves, France) and two filters, is placed into the Optem 125C objective. This cube allows to collect the emitted fluorescence in the same axis without background "noise" by separating the excitation and emission light components. The dichroic mirror has a transition wavelength value of 532 nm. A laser line filter is placed on the excitation path prior to the dichroic mirror in order to select the excitation wavelength (532 nm ± 10 nm). A more specific selection of the light emitted from the sample is obtained using an emission filter placed beneath the dichroic mirror (high-pass filter > 540 nm).

Fluorescence spectra of fluorescent dyes from the ESI plume were recorded by an ultra-compact Econic spectrophotometer (B&WTek Inc., Newark, DE, USA). This spectrophotometer consists of a monochromator with a diffraction grating and a CCD array and allows dispersing spatially the fluorescence signal as a function of the wavelength with a resolution of 1.5 nm (thanks to a 25 μm entrance slit). The spectrometer is directly fixed to the Optem 125C objective and cooled to 5 °C using an external oil circulator device (Haake Phoenix II P1, Thermo Scientific, Karlsruhe, Germany) and a brass tank surrounding the spectrophotometer. When the CCD is cooled down to 5 °C, the dark current is reduced by a factor ~4.

The excitation laser, the spectrophotometer and all the optics (objectives, mirrors filters and fluorescence cube) are mounted onto a moving stage. Three step-by-step motors (LMS 80, OWIS) allow the *X*, *Y* and *Z* moves and the scanning of the ESI plume with a precision that can be better than 4 μm. We use a home-developed, VISUAL C++, Windows-based software controlling the moving stage and the data acquisition. This home-made software first allows the piloting of the moving stage on *X*, *Y* and *Z* axis for a specific positioning as well as the automatic step-by-step move for the 3D profiling. The exposition time and averaged scans of the spectrophotometer can be adjusted via the software interface. In the profiling mode, the spectrophotometer is synchronized with the motors and fluorescence spectra are recorded at each step.

2.2. Mass spectrometry

Experiments were performed on a Single Quad 6100 equipped with a modified Agilent Jet Stream ESI source (Agilent Technologies, Santa Clara, CA, USA). The commercial AJS-ESI source has been modified in order to allow the laser injection into the plume and the epifluorescence measurements. For that, 40 mm-diameter holes

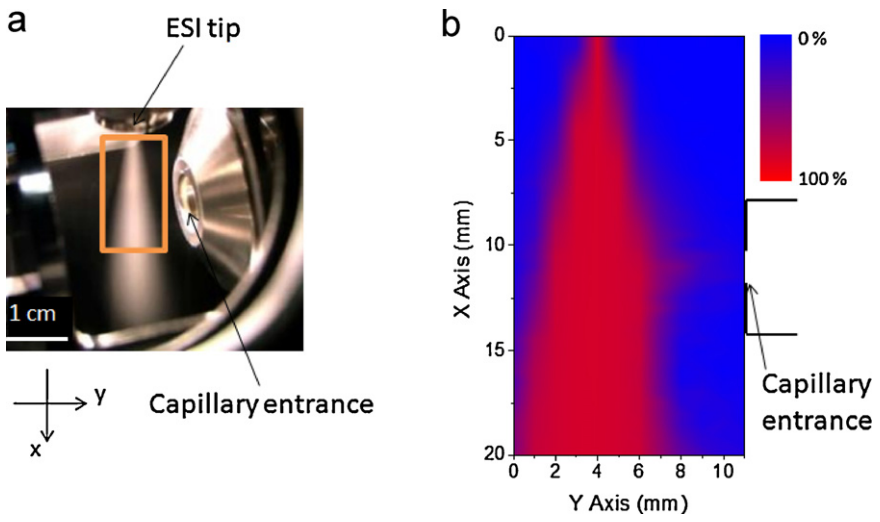

Fig. 2. (a) Picture of the illuminated ESI plume. The rectangle corresponds to the scanned area of the plume for fluorescent measurements (X = 0–20 mm, Y = 0–11 mm and Z was set at the entrance of the capillary). (b) XY images of the relative fluorescence signal of 1×10^{-5} M Rh6G in MeOH/water 80:20 (%, v/v) in the plume. The irradiation time for each step was set to 5 s. The image is constituted of 943 points and the total acquisition time for an image is 4715 s. The spray was produced in positive mode with a solution of 1×10^{-5} M Rh6G in MeOH/water 80:20 (%, v/v) infused at 50 μL/min and ionization parameters were: SGF = 7 L/min, SGT = 180 °C. The position of the tip of the electrospray needle is X = 0 mm, Y = 4 mm, the position of the capillary entrance of the MS (which is shown) is X = 12 mm.

have been drilled in both sides of the AJS-ESI source. The hole centers are placed third way between the capillary axis and the exit of the nebulizer in the vertical direction. The holes are lined up with the nebulizer in the horizontal direction.

Nitrogen was used as the nebulizing gas (25 psi), the drying gas (4 L/min, 250 °C) and super-heated sheath gas. The sheath gas flow rate and temperature were set according to the experiments. The ionization source was operated in negative and positive ion modes with the capillary voltage set at −2000 V or +3000 V and the nozzle voltage at −1200 V or +800 V, respectively. The Agilent ChemStation software provided by Agilent Technologies was used for instruments control, data acquisition and data processing.

2.3. Chemicals

The fluorescent pH indicator 5 (and 6)-[10-(dimethylamino)-3-oxo-3H-benzo[c]xanthenes-7-yl]benzenedicarboxylic acid dye (C.SNARF-1) was purchased from Invitrogen Molecular Probes (Cergy Pontoise, France). Other chemicals were obtained from Sigma–Aldrich (Saint Quentin Fallavier, France). All solutions were aqueous, using milli-Q water (18.2 MΩ cm). C.SNARF-1 solutions were prepared by dilution of a stock solution (2 mM) to a final 250 μM concentration. The initial pH of C.SNARF-1 solutions was 5.58. Solutions of 250 μM C.SNARF-1 at different pH values were prepared by diluting a stock solution with water. The pH was adjusted by adding 1 mM NaOH prior to final dilution. The pH of solutions was measured using a 211R pHmeter equipped with a 4 mm-diameter microelectrode (Hanna Instruments, Woonsocket, RI, USA). In order to correlate the pH in the ESI plume to the MS signal, peptides were added in the sprayed solutions at a 200 μM concentration. Oxytocin and Angiotensin II (Sigma–Aldrich, Saint Quentin Fallavier, France) were used as received.

Rhodamine 6G (Rh6G) was purchased from Lambda Physik (Lauderdale, FL, USA). This Rh6G was dissolved in methanol (MeOH) and further diluted in a MeOH/water 80:20 (%, v/v) binary mixture to a final 10 μM concentration.

Solutions were introduced in the ionization source at 50 μL/min flow rate with a KDS100 syringe pump (KD Scientific, Holliston, MA, USA).

2.4. Optical profiling. Procedure, sensitivity and resolution

For initial assessment of the profiling capabilities of the system, it was desired to establish the spatial resolution and the sensitivity of our optical set-up. For this purpose, we used Rhodamine 6G (Rh6G). It is a non-chromic dye having a good solubility in MeOH and absorbing at 532 nm and has a fluorescence quantum yield of 95% in MeOH.

The spatial resolution depends on the laser beam diameter and the resolution of the optics. To characterize this resolution, we used a calibration cell containing a methanolic solution of Rh6G at 1.5 μM. The X, Y and Z axis were scanned point-by-point with a step size of 0.1 mm and a fluorescence spectrum was recorded at each point. The cell is a 10 mm quartz cuvette with 1 mm-thick walls. The fluorescence signal at 550 nm (corresponding to Rh6G) is insignificant when the laser is outside the cell. It radically increases as the laser reaches the calibration cell. The resolution can be calculated from the derivatives of the fluorescence signal against the axial position. The spatial resolution (on X and Y axis) for the fluorescence set-up is 200 μm. The same protocol has been used to determine the spatial resolution on the Z axis which is around ∼1 mm. The field of view in depth (i.e., Z axis) is higher due to the collecting optics, leading to a worse resolution on the Z axis.

In order to evaluate the sensitivity of the optical detection, in particular the limit of detection (LOD), fluorescence signal was recorded using solutions of Rh6G at different concentrations. An example of plume images obtained with a solution of Rh6G at 10 μM in MeOH/water 80:20 (%, v/v) is shown in Fig. 2. The solution was infused continuously with a syringe-pump, while the ESI plume was scanned by the laser beam. 2D XY profile maps of the AJS ESI plume has been obtained by recording the fluorescence signal of the Rh6G at 550 nm. The Z axis was centered on the capillary entrance and the dimension of the XY images was 20 mm × 11 mm (area presented on the picture of the illuminated ESI plume in Fig. 2a) with a step of 500 μm in both directions. The irradiation time at each step was set to 5 s. The image presented in Fig. 2b is constituted by 943 points and the total acquisition time for an image is 4715 s. The signal is maximum on the axis of the needle. We can also see the focalization of some Rh6G ions toward the capillary entrance at X = 12 mm. We can note that the ESI profile changes in dimension for different sheath gas flows (SGF) and

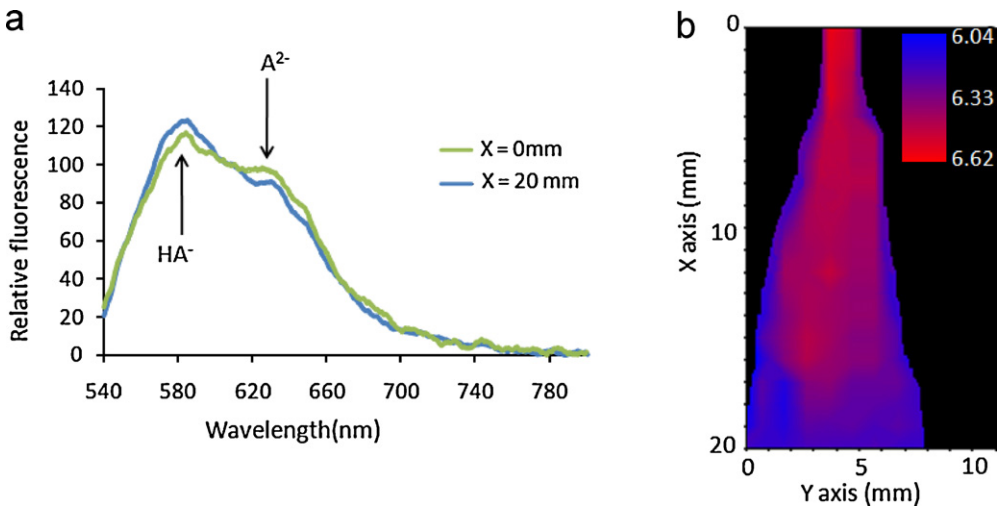

Fig. 3. (a) Fluorescence spectra obtained by spraying a 250 μM C.SNARF-1 aqueous solution at an initial pH of 6.5 in the negative ion mode at $X = 0$ mm and 20 mm. The spectra were normalized to the isoemissive point at 607 nm. The irradiation time was set to 5 s. The sheath gas parameters were: SGF = 7 L/min, SGT = 180 °C. (b) *XY* image of the pH in the plume (from the fluorescence of 250 μM C.SNARF-1 in water at an initial pH of 6.5). The irradiation time for each step was set to 5 s. The image is constituted of 943 points and the total acquisition time for an image is 4715 s. The sheath gas parameters were SGF = 7 L/min, SGT = 180 °C.

temperatures (SGT) (data not shown). The ESI plume is thinner as the sheath gas flow increases because of the spray confinement. The evaporation of droplets within the spray is more efficient when the temperature of the sheath gas is higher, which results in a thinner spray.

To determine the limit of detection (LOD), methanolic solutions of Rh6G at 10^{-8} M, 10^{-9} M, 10^{-10} M and 10^{-11} M were infused at 50 μL/min and the fluorescence signal of Rh6G at 550 nm was measured at the center of the ESI plume. The limit of detection for fluorescence measurements was estimated at 10^{-11} M (at this concentration the signal-to-noise ratio is ~1.33). The LOD is limited by the irradiation volume of dye solution in the ESI plume. The beam waist at the focus spot is around 0.1 mm, and the estimated interrogation volume is $\sim 10^{-2}$ mm^3. Thus, our LOD corresponds roughly to 6×10^4 Rh6G molecules. The dynamic range of detection is the ratio between the concentration corresponding to the LOD and the highest possible concentration in dyes for which fluorescence spectra are not saturated. It was estimated to 10^4.

3. Results and discussion

3.1. Profiling the plume pH

C.SNARF-1 is a pHchromic dye (the structure can be found in the inset in Fig. S1b in the Supporting Information). pH-chromism is due to differences in fluorescence spectra of a dye between its basic and acid forms. The fluorescence of a solution is a combination of the fluorescence spectra of the acid and basic forms and depends on the relative concentration of the two forms and then on the pH. The doubly (A^{2-}) and singly (HA^-) deprotonated species are the fluorescent forms of this indicator [18]. The pKa relevant to the fluorescent forms of C.SNARF-1 is 7.5 [18], making it suitable for measuring pH around 7.5 ± 1. First of all, the chromism of this dye was calibrated at various pH values (see Section 2). The UV–Vis emission spectra of 250 μM C.SNARF-1 in aqueous solutions at different pH are shown in Fig. S1a. Fluorescence spectra are characterized by two emission bands corresponding to the acid species and the basic species. The acid HA^- and basic A^{2-} fluorescence signals are located at $\lambda = 587$ nm at pH 6.0 and $\lambda = 638$ nm at pH 8.5, respectively. In addition, the maximum emission wavelengths of HA^- and A^{2-} show small shifts as the pH decreases due to chromic effects, which is consistent with reported literature [19]. Because the AJS source operates with a sheath gas of 180 °C, the spray droplets may be hotter than room temperature. Hence, the potential effect of the temperature on the fluorescence behavior of C.SNARF-1 has been evaluated. The fluorescence spectra of solutions at 40 °C and 80 °C did not differ significantly from those obtained at 20 °C (see Fig. S2 in the Supporting Information), suggesting that the effect of temperature on spectroscopic properties of C.SNARF-1 is small [20]. The pH of a C.SNARF-1 solution can then be determined based on the two species fluorescence intensity ratio $\log(I_{A^{2-}}/I_{HA^-})$ (where I is the intensity at the maximum of each fluorescence band) using the calibration curve deduced from Fig. S1b.

Fluorescence spectra acquired from the spray at $X = 0$ mm and 20 mm (with $Y = 4.0$ mm corresponding to the exit of the tip emitter) obtained by electrospraying, in negative mode an initial solution of C.SNARF-1 at pH 6.5 (pH adjusted with 4×10^{-5} M of NaOH) with a sheath gas flow set at 7 L/min and a temperature of 180 °C are shown in Fig. 3a. The arrows in Fig. 3a highlight the increase in emission attributable to the singly deprotonated form of the dye (HA^-, emitting at $\lambda = 588$ nm) as the X increases and the corresponding decrease of the doubly deprotonated form (A^{2-}, $\lambda = 635$ nm). 2D *XY* maps of the pH within the ESI plume were obtained from the recorded fluorescence signal of C.SNARF-1 at each point. The pH values, obtained using the calibration curve, are plotted on the 2D map in Fig. 3b. The results clearly indicate that the pH within the droplets is not homogeneous in the ESI plume. The pH of the droplets decreases as they move down the plume. Furthermore, the lateral heterogeneity is also clearly evident from the image in Fig. 3b. The pH is lower at the edge of the spray plume than at the center.

pH values on the axis of the plume as a function of distance X from the emitter tip for different initial pH solutions are also plotted in Fig. 4a. The error on the pH values depends on the accuracy of the fluorescence measurements. This error can be estimated by calculating a standard deviation based on three replicates of the fluorescence signal measurement at each point. This error is ranging from ±0.01 to ±0.03 pH units (note that the precision on the pH values of the initial solutions with the commercial pHmeter is ±0.01). The large errors observed far from the emitter tip are due to the global decrease in the fluorescence signal along the X axis, which yields to a lower accuracy on the ratio of $\log(I_{A^{2-}}/I_{HA^-})$. The error reported for the lowest and highest pH values reflects measurements beyond the optimum pH range of the C.SNARF-1 dye.

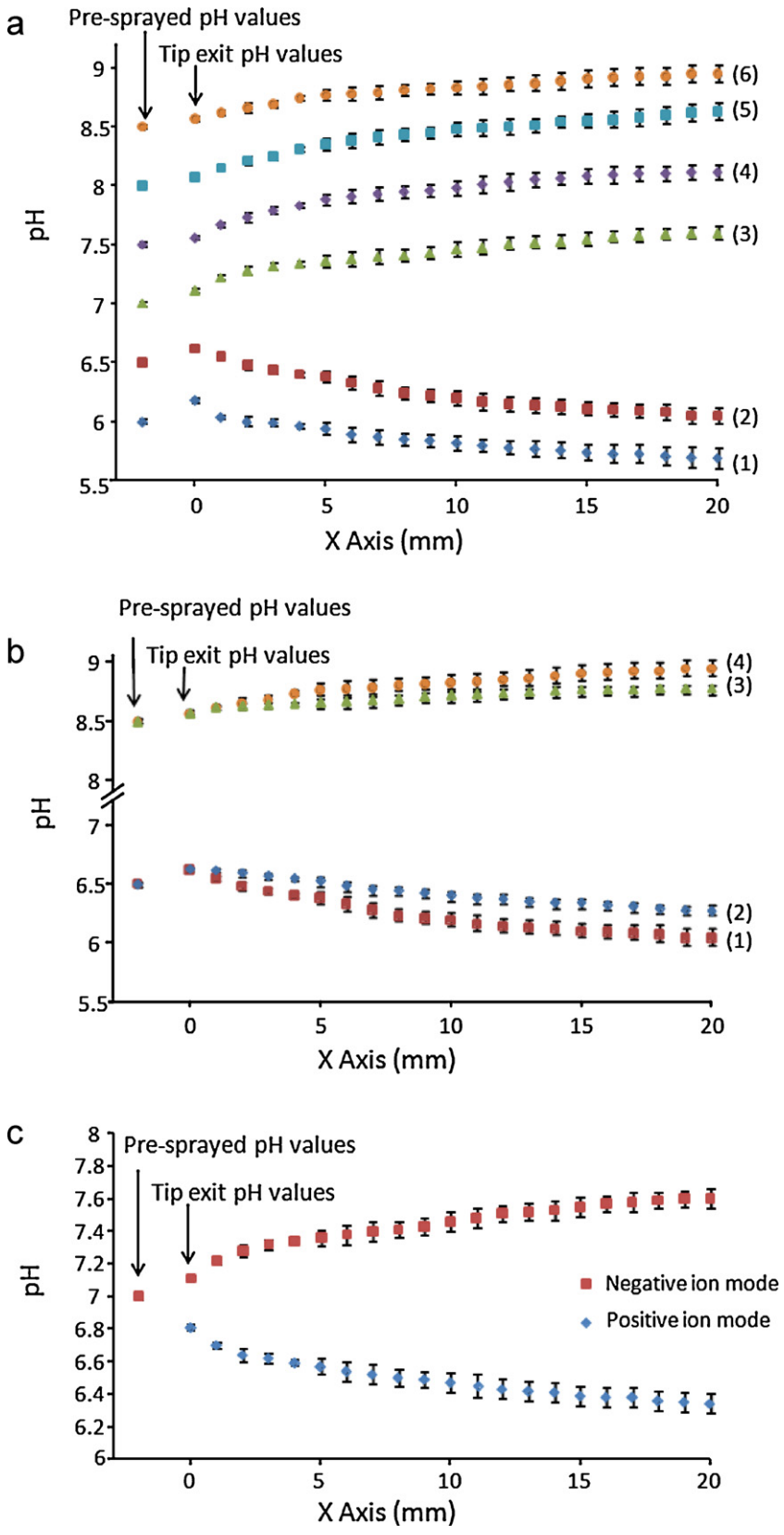

Fig. 4. Plots of the pH values determined from the fluorescence spectra of 250 μM C.SNARF-1 in the spray plume versus the axial distance *X* from the emitter tip. The leftmost point in each plot reports the pH of the bulk solution prior to spraying. (a) Initial pH values: curve (1), 6.0; curve (2), 6.5; curve (3), 7.0; curve (4), 7.5; curve (5), 8.0; curve (6), 8.5. The ionization parameters were: SGF = 7 L/min, SGT = 180 °C, capillary voltage = −2 kV in negative mode for all the curves. (b) Initial pH values: curves (1) and (2), 6.5; curves (3) and (4), 8.5. The ionization parameters were: curves (1) and (4) SGF = 7 L/min, SGT = 180 °C; curves (2) and (3) SGF = 0.2 L/min, SGT = 25 °C, capillary voltage = −2 kV in negative mode. (c) Initial pH values: 7.0 for all curves. The ionization parameters were: SGF = 7 L/min, SGT = 180 °C, capillary voltage = +3 kV in positive mode; capillary voltage = −2 kV in negative mode.

Evolution of the pH along the plume starting from different initial solutions (see Fig. 4a) is discussed in details below. We can first notice that the pH measured at the exit of the emitter tip ($X = 0$ mm) differs from the initial pH of the pre-sprayed solutions. The small pH increase at the exit of the tip is due to the electrolytic generation of OH^- by solvent reduction in the negative ion mode. This effect can be quantitatively estimated from the spray current, assuming that every electron injected in the negative-ion mode generates hydroxide ions (reduction of water, $2H_2O + 2e^- \rightarrow 2OH^- + H_2$) [21]. The relevant concentration of the electrolytically generated $[OH^-]_e$ can be estimated by $[OH^-]_e = i_{ES}/_{Fvf}$ where i_{ES} is the ESI current, F is the Faraday constant (9.648×10^4 C mol^{-1}), and v_f is the volumetric flow rate of solution through the emitter. The final pH at the exit of the tip can then be estimated, using the known pKa values of C.SNARF1 (7.5), as described in details previously [8]. The final pH values predicted in this way are presented in Table ST1 in the Supporting Information for solutions with different initial pH values. Agreement between the calculated and the measured pH values is good. The data clearly indicate that the majority of the electrolysis current is provided by reduction of water.

Then along the plume, depending on the initial value of the pH, two opposite evolutions are observed for the pH of droplets as they move down the plume. For initial pH > 7, the pH of the droplets increases, while for pH < 7, the pH continuously decreases (Fig. 4a). For acidic initial solutions (pH < 7), the decrease is consistent with the intuitive expectation that the pH of an acidic solution should drop as the volume decreases and the acid species become more concentrated due to the solvent evaporation. The increase in proton concentration is related to the decrease in the droplet volume along the spray plume. When volatile solvents are involved and the droplets are a few micrometers in diameter, the evaporation rate follows the surface evaporation limit law which leads to a simple dependence of the droplet radius on time t [22,23] ($R = R_0 - 9.96 \times 10^{-5} t$, for water droplets at 300 K). Assuming an initial droplet diameter of 10 μm, and a droplet velocity of ~1 m/s [24], evaporation of droplets leads to ~5-fold decrease in the volume, at 20 mm. pH after evaporation is then calculated from the known initial concentration of the different ions in solution (in particular of C. SNARF-1) and the pKa value. Starting with a pH at 6.63 leads to a final pH = 6 at 20 mm in qualitative agreement with the observed pH evolution in Fig. 4a. Note that the pH evolution depends on the estimation of the initial value of the droplet diameter and its velocity (see Fig. S3 in the Supporting Information). In the same way, for initial basic solutions (pH > 7), the solution is expected to become more basic as a result of solvent evaporation. Similar calculations explain the increase in pH for initial solutions with pH > 7 as observed in Fig. 4a. This result is opposite to Cook's work, where the pH value slightly decreased at the further positions along the axis of the plume when the initial pH was basic [10]. In our case, the use of a heated sheath gas which allows a better evaporation process could possibly explain this difference. Thus, experiments were conducted with a sheath gas flow rate set at 0.2 L/min and a temperature of 25 °C in order to probe this effect. Fig. 4b shows plots of the pH values versus the axial distance for initial pH of 6.5 and 8.5 with optimal (curves 1 and 4) and with minimum (curves 2 and 3) sheath gas conditions. The pH increase along the X axis is much lower when the sheath gas temperature is 25 °C (0.23 for SGT = 25 °C instead of 0.67 for SGT = 180 °C). The heated sheath gas allows a better concentration of the basic species within the droplet as a result of the enhanced evaporation process. Similar results are obtained when spraying a solution with initial pH 6.5 (curves 1 and 2 in Fig. 4b). The fluorescence of C.SNARF-1 is also affected by aggregation for concentrations above 1 mM [20]. The difference in C.SNARF-1 concentrations between the two studies may also play a role in the pH change profiles, although the initial concentration of 250 μM was below this threshold and did probably not induce aggregation of the dye during the shrinking process of droplets. To probe this assumption, experiments were performed with a 50 μM initial concentration of dye and the same evolution of the pH of droplets along the X axis, for both initial acid and basic pH, were observed (see Fig. S4 in the Supporting Information). An important finding in this work is that, since for pH < 7, the pH along the plume decreases and on the other hand, for pH > 7, the pH increases, it means that droplets at the end of the plume for unbuffered solutions do not have pH between 6.6 and 7.2. On the other hand, for buffered solutions of C.SNARF-1, the pH values in the spray do not change neither at the tip emitter nor along the spray plume (see Fig. S5 in Supporting Information). In fact, the excess of buffer in the solutions prevents apparition of these effects in the spectra.

In addition, the pH change within the droplets has been compared when spraying a solution with initial pH 7.0 in the negative and the positive ion mode (Fig. 4c). In contrast to the negative ion mode (curve 2), the pH decreases when spraying the solution in the positive ion mode (curve 1). Indeed, the pH measured at the exit of the emitter tip had decreased to 6.81 due to the electrolytic generation of protons by solvent oxidation in the positive ion mode [8]. The droplets are then acid and become more acid due to the evaporation process. In the positive mode, our results are very similar to those reported by Cook and coworkers [10].

3.2. Influence of the sheath gas parameters and correlation with the MS signal

The ESI Agilent Jet Stream thermal gradient focusing source was developed to significantly improve the desolvation process thanks to the super-heated sheath gas [25]. The influence of the sheath gas parameter on the pH in the ESI plume and on the peptide MS signal has been investigated. Fig. 5a shows the plots of pH values in the spray plume versus the axial distance X from the emitter tip for different sheath gas flow rates and temperatures and an initial solution of pH 8.5. The pH within the droplets depends on the concentration of each component in the mixture, which is governed as discussed above by the solvent evaporation process. In our case for initial pH 8.5, the evaporation of solvent during the shrinking of the ESI droplets yields to more basic droplets in the downstream droplets and the droplets at the edge of the spray which are exposed to the sheath gas. The sheath gas flow rate induces a change in pH values due to changes in the desolvation process. The evaporation of droplets within the spray is more efficient when the sheath gas flow is higher. As shown in Fig. 5a, this yields a higher evaporation rate of solvent and more basic droplets far away from the ESI emitter. Indeed, for a sheath gas flow of 5 L/min the difference between the pH at $X = 20$ mm and $X = 0$ mm is 0.64, while this pH change is 0.67 for a sheath gas flow of 7 L/min. As shown previously, the temperature of the sheath gas also plays a role on the droplet evaporation. Indeed, the pH change along the X axis is higher when the sheath gas temperature is higher (0.67 for SGT = 180 °C and 0.69 for SGT = 210 °C, Fig. 5a). The heated N_2 sheath gas helps to improve the droplet evaporation during the ESI process, and can change the droplet chemical properties [25].

The pH profiles obtained for different sheath gas flow rates and temperatures have been correlated with the MS signal of oxytocin ions recorded during the image acquisition, which is unique as compared to previously reported results. The ESI-MS signal is very stable during the 4715 s of the image acquisition and the standard deviation of the total ion current is only 0.5%. In negative ion mode and basic pH condition, oxytocin is observed as a singly deprotonated ion $[M-H]^-$ at m/z 1006, a doubly deprotonated ion $[M-2H]^{2-}$ at m/z 502 and a triply deprotonated ion $[M-3H]^{3-}$ at m/z 335 (ESI-MS spectrum of oxytocin for an initial solution of pH 8.5 is presented in Fig. S6a). The relative intensities of these charge states are modified according to the sheath gas parameters, as

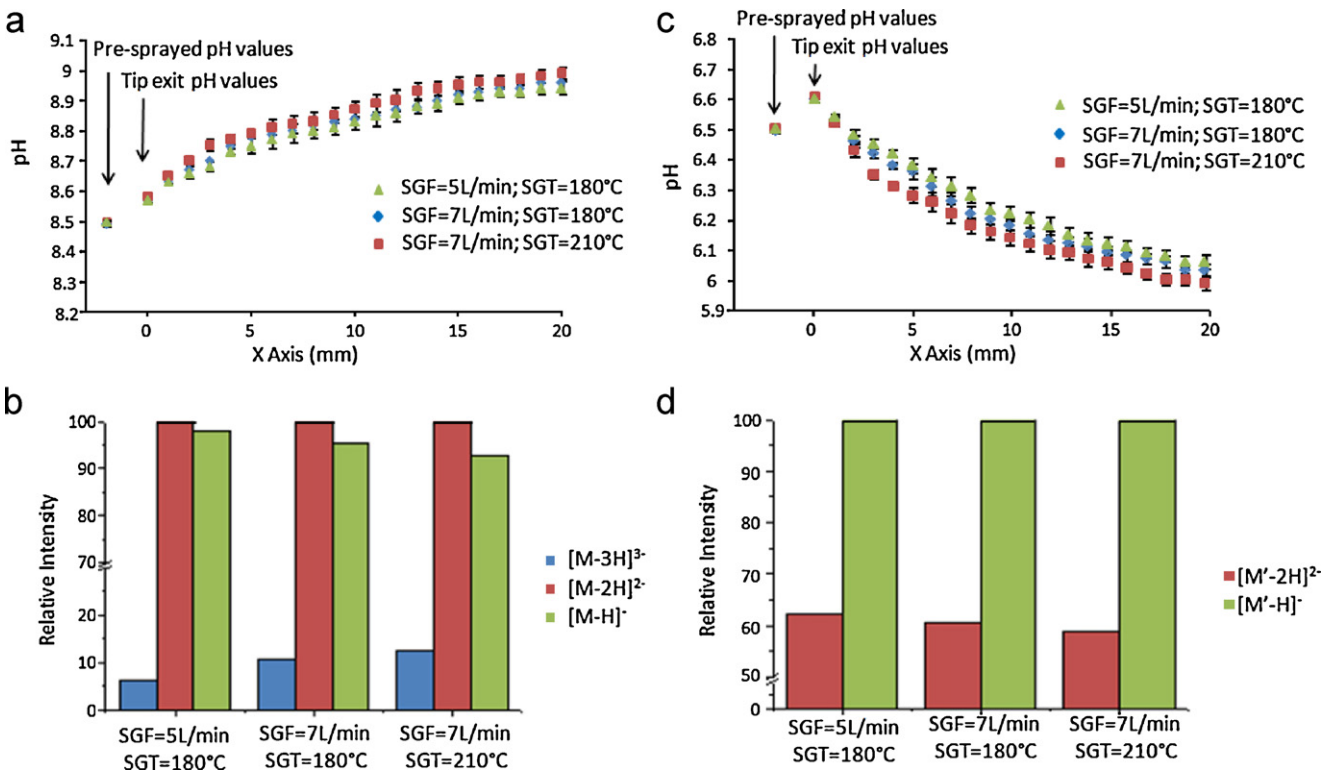

Fig. 5. (a) Plots of pH values in the spray plume versus the axial distance *X* from the emitter tip (at *Y* = 4 mm and *Z* at the entrance of the capillary) for different sheath gas flow rates and temperatures and an initial solution of pH 8.5. Sheath gas parameters were: (▲) SGF = 5 L/min, SGT = 180 °C; (♦) SGF = 7 L/min, SGT = 180 °C and (■) SGF = 7 L/min, SGT = 210 °C. (b) Relative intensities of oxytocin ions (three charge states), for the same different sheath gas flow rates and temperatures and an initial solution of pH 8.5, observed in negative ion mode MS. (c) Plots of pH values in the spray plume versus the axial distance *X* from the emitter tip (at *Y* = 4 mm and *Z* at the entrance of the capillary) for different sheath gas flow rates and temperatures and an initial solution of pH 6.5. Sheath gas parameters were: (▲) SGF = 5 L/min, SGT = 180 °C; (♦) SGF = 7 L/min, SGT = 180 °C and (■) SGF = 7 L/min, SGT = 210 °C. (d) Relative intensities of angiotensin II ions (two charge states) for the same different sheath gas flow rates and temperatures and an initial solution of pH 6.5, observed in negative ion mode MS.

shown in Fig. 5b. When the droplet evaporation efficiency increases (i.e., higher sheath gas flow and temperature), the relative intensity of the $[M-3H]^{3-}$ ion also increases while the relative intensity of the $[M-H]^{-}$ ion decreases. These results are directly correlated to pH droplets measurements. Indeed, higher pH values observed for final droplets (downstream values) result in the most efficient deprotonation of oxytocin. Oxytocin (OT) is a peptide without carboxyl groups [23]. The most acidic group in OT is the Tyr2 side chain (pKa ~10.0–10.3) [26]. The first deprotonation site is then expected to be the OH group of Tyr2. The other proton-containing groups, the –CONH– backbone amides, the $–CONH_2$ amides of Gln4, Asn5, and Gly9, and the N-terminal $–NH_2$ amino group, have significantly higher p*K*a values. The pK value of the terminal amino group is significantly lowered as compared to the other groups [27] due to the close vicinity of the disulfide group. The second deprotonation may then occur at the terminal amino group. The third deprotonation could occur on the peptide backbone (nitrogen atom of the amide bond, pKa > 13) [27]. At *X* = 20 mm the pH raises ~9.1, which is not enough to explain the observed amount of $[M-3H]^{3-}$. Indeed, at pH = 9, the ratio between 2- and 3-abundance ions is $<10^{-4}$ (10^{pH-pKa}). The 3-/2-ratios observed in mass spectra ($\sim10^{-1}$) is much higher and is due to a significant increase in the pH in droplets during the ultimate desolvation process (which cannot be monitored in our current ESI profiling). In conclusion, the relative abundance observed for the 3-charge state ions is related to the droplet pH at the end of the spray and not only to the pH of the initial solution. This also explains results previously reported for peptide charge state distributions in positive mode ESI-MS [7,28].

The same experiments have been made for a solution of initial pH 6.5 containing the C.SNARF-1 pH indicator and angiotensin II. The plots of pH values in the spray plume versus the axial distance *X* from the emitter tip for different sheath gas flow rates and temperatures and a constant initial solution of pH 6.5 are presented in Fig. 5c. In agreement with the results shown in Fig. 3, Fig. 5c shows that more acid droplets are produced when spraying the solution with higher sheath gas flow rate and temperature due to the improvement in the evaporation process. The relative intensity of singly deprotonated ion $[M'-H]^{-}$ of angiotensin II detected at *m*/*z* 1045 and the doubly deprotonated ion $[M'-2H]^{2-}$ of angiotensin II detected at *m*/*z* 522 change according to the sheath gas parameters, as shown in Fig. 5d. In this case, the relative intensity of the $[M-2H]^{2-}$ ion is lower when a 7 L/min flow rate and a 210 °C temperature are used. This is opposite to what is observed for an initial solution with pH > 7 (see Fig. 5b) and is in agreement with the pH evolution observed in both cases.

4. Conclusion

In summary, we implemented a laser-induced-fluorescence profiling set-up on a modified Agilent Jet Stream electrospray source coupled to a single quadrupole mass analyser. Using a pH-chromic dye, this coupling allowed simultaneous measurements of mass spectra and optical pH profiles and permitted to study the relation between the observed charge state of peptide anions and pH changes in the spray plume. We showed that improvement of desolvation processes for initial solution with pH > 7 induces an increase in droplets pH and favors high negatively charges in mass spectra. On the other hand, desolvation for initial solution with pH < 7 results in a decrease in droplets pH and favors low negatively charges in mass spectra. Charge states in mass spectra for

peptide anions are controlled by the pH of the droplets at the end of the plume before transfer to the gas phase.

Charge-state distributions of gas-phase ions from proteins and their noncovalent complexes are increasingly used to gauge their conformations in the solution phase. It is clear that a combination of MS measurements and pH profiling along the plume would help to better investigate the correlation between charge-state distributions and conformation. Obviously, the dynamics of the ESI process is complex and determination of other physico-chemical parameters, such as temperature and size of droplets, is required for a better understanding of the transition from solution-phase to gas-phase ions. Work along these lines is currently underway in our laboratory.

Supporting information

Additional supporting information may be found in the online version of this article: estimation of pH at the ESI tip emitter for negative-ion electrospray of unbuffered C.SNARF-1 sprayed solutions (Table ST1), fluorescence spectra of 2C.SNARF-1 at different pH and calibration curve (Fig. S1) and at different temperatures (Fig. S2), theoretical plots of the pH value evolution along the spray plume (Fig. S3), plots of the pH values determined from the fluorescence spectra of C.SNARF-1 at initial concentrations of 250 μM and of 50 μM (Fig. S4), plots of the pH values determined from the fluorescence spectra of buffered solutions of C.SNARF-1 in the spray plume (Fig. S5), negative ion mode ESI-MS spectra of oxytocin and angiotensin II (Fig. S6), Fluorescence spectra of C.SNARF-1 in unbuffered water at different concentrations (20 μM and 250 μM) for pH 6.5 and pH 8.0 (Fig. S7), Plots of the pH values determined from the fluorescence spectra of 250 μM C.SNARF-1 with and without oxytocin peptide in solution (Fig. S8).

Acknowledgements

This work was supported by Agilent Technologies with an award through Agilent's Application and Core Technology University Research Program (Grant ID 2243). Mark Werlich and Alex Mordehai are acknowledged for their assistance for the Agilent Jet Stream ESI source modifications. The authors would like to thank David Lascoux for helping initiating the project. Jacques Maurelli and Jad Tabbara are acknowledged for their invaluable technical assistance.

Appendix A. Supplementary data

Supplementary data associated with this article can be found, in the online version, at doi:10.1016/j.ijms.2011.07.020.

References

[1] J.B. Fenn, M. Mann, C.K. Meng, S.F. Wong, C.M. Whitehouse, Electrospray ionization for mass spectrometry of large biomolecules, Science 246 (1989) 64.
[2] R.B. Cole, Electrospray Ionization Mass Spectrometry: Fundamentals, Instrumentation and Applications, Wiley-Interscience, New York, 1997.
[3] T.C. Rohner, N. Lion, H.H. Girault, Electrochemical and theoretical aspects of electrospray ionisation, Phys. Chem. Chem. Phys. 6 (2004) 3056.
[4] G.J. Van Berkel, V. Kertesz, Using the electrochemistry of the electrospray ion source, Anal. Chem. 79 (2007) 5510.
[5] P. Kebarle, U.H. Verkerk, Electrospray: from ions in solution to ions in the gas phase, what we know now, Mass Spectrom. Rev. 28 (2009) 898–917.
[6] P. Kiselev, J. Rosell, J.B. Fenn, Ind. Eng. Chem. Res. 36 (1997) 3081.
[7] X.F.D. Chillier, A. Monnier, H. Bill, F. Gulacar, A. Buchs, S.A. McLuckey, G.J. Van Berkel, A mass spectrometry and optical spectroscopy investigation of gas-phase ion formation in electrospray, Rapid Commun. Mass Spectrom. 10 (1996) 299.
[8] S. Zhou, A.G. Edwards, K.D. Cook, G.J. Van Berkel, Investigation of the electrospray plume by laser-induced fluorescence spectroscopy, Anal. Chem. 71 (1999) 769.
[9] S. Zhou, K.D. Cook, Probing solvent fractionation in electrospray droplets with laser-induced fluorescence of a solvatochromic dye, Anal. Chem. 72 (2000) 963.
[10] S. Zhou, B.S. Prebyl, K.D. Cook, Profiling pH changes in the electrospray plume, Anal. Chem. 74 (2002) 4885.
[11] D. Davis, E. Portelius, Y. Zhu, C. Feigerle, K.D. Cook, Profiling an electrospray plume using surface-enhanced Raman spectroscopy, Anal. Chem. 77 (2005) 8151.
[12] K. Chingin, V. Frankevich, R.M. Balabin, K.V. Barylyuk, H.W. Chen, R. Wang, R. Zenobi, Direct access to isolated biomolecules under ambient conditions, Angew. Chem., Int. Ed. 49 (2010) 2358.
[13] R. Wang, R. Zenobi, Evolution of the solvent polarity in an electrospray plume, J. Am. Soc. Mass Spectrom. 21 (2010) 378.
[14] A. Wortmann, A. Kistler-Momotova, R. Zenobi, M.C. Heine, O. Wilhelm, S.E. Pratsinis, Shrinking droplets in electrospray ionization and their influence on chemical equilibria, J. Am. Soc. Mass Spectrom. 18 (2007) 385.
[15] L. Konermann, D.J. Douglas, Acid-Induced Unfolding of Cytochrome c at Different Methanol Concentrations: Electrospray Ionization Mass Spectrometry Specifically Monitors Changes in the Tertiary Structure, Biochemistry 36 (1997) 12296.
[16] S.E. Rodriguez-Cruz, J.T. Khoury, J.H. Parks, Protein fluorescence measurements within electrospray droplets, J. Am. Soc. Mass Spectrom. 12 (2001) 716.
[17] S. Ideue, K. Sakamoto, K. Homma, D.E. Clemmer, Conformational change of electrosprayed cytochrome c studied by laser-induced fluorescence, Chem. Phys. Lett. 337 (2001) 79.
[18] J.E. Whitaker, R.P. Hauglan, F.G. Prendergast, Spectral and photophysical studies of benzo[c]xanthene dyes: dual emission pH sensors, Anal. Biochem. 194 (1991) 330–344.
[19] A. Timperman, S.E. Tracht, J.V. Sweedler, Dynamic on-column pH monitoring in capillary electrophoresis: application to volume-limited outlet vials, Anal. Chem. 68 (1996) 2693–2698.
[20] J.W. Parker, O. Laksin, C. Yu, M.L. Lau, S. Klima, R. Fisher, I. Scott, B.W. Atwater, Fiber-optic sensors for pH and carbon dioxide using a self-referencing dye, Anal. Chem. 65 (1993) 2329–2334.
[21] G.J. Van Berkel, F. Zhou, J.T. Aronson, Changes in Bulk Solution pH Caused by the Controlled-Current Electrolytic Process Inherent to Operation of an Electrospray Ion Source, Int. J. Mass Spectrom. Ion Process. 162 (1997) 55–67.
[22] P. Kebarle, L. Tang, From ions in solution to ions in the gas phase - the mechanism of electrospray mass spectrometry, Anal. Chem. 65 (1993) 972A.
[23] D.C. Taflin, T.L. Ward, E.J. Davis, Electrified droplet fission and the Rayleigh limit, Langmuir 5 (1989) 376.
[24] P. Nemes, I. Marginean, A. Vertes, Spraying Mode Effect on Droplet Formation and Ion Chemistry in Electrosprays, Anal. Chem. 79 (2007) 3105–3116.
[25] A. Mordehai, ESI Technology with thermal gradient focusing – theoretical and practical aspects, in: Proceedings of the 57th ASMS Conference on Mass Spectrometry & Allied Topics, Philadelphia, Pennsylvania, 2009.
[26] L. Joly, R. Antoine, A.-R. Allouche, M. Broyer, J. Lemoine, P. Dugourd, Optical properties of isolated hormone oxytocin dianions: ionization reduction, and copper complexation effects, J. Phys. Chem. A 113 (2009) 6607.
[27] H. Sigel, R.B. Martin, Coordinating properties of the amide bond. Stability and structure of metal ion complexes of peptides and related ligands, Chem. Rev. 82 (1982) 385.
[28] R.B. Wang, G. Cole, Disparity between solution-phase equilibria and charge state distributions in positive-ion electrospray mass spectrometry, Org. Mass Spectrom. 29 (1994) 419–427.